ELSEVIER

Aerosol Science 35 (2004) 707–730

Journal of
Aerosol Science

www.elsevier.com/locate/jaerosci

Monte-Carlo simulation of unipolar diffusion charging for spherical and non-spherical particles

G. Biskos*, E. Mastorakos, N. Collings

Hopkinson Laboratory, Department of Engineering, University of Cambridge, Trumpington Street, Cambridge CB2 1PZ, UK

Received 10 August 2003; received in revised form 27 November 2003; accepted 28 November 2003

Abstract

This paper presents a 3D Monte-Carlo model that simulates diffusion charging of aerosol particles in positive unipolar environments. Calculations are performed for $N_i t$ products up to 5×10^{12} ions m^{-3} s (with N_i being the ion concentration and t the charging time), and particles with diameter 5–1000 nm, covering a wide range of Knudsen numbers at atmospheric pressure. Apart from the average charge, the code allows for the calculation of the charge distribution which is shown to be well described by Gaussian statistics for monodisperse particles. Standard deviations of the charge distribution calculated with the source-and-sink approach show good agreement with the Monte-Carlo results. Comparison of the Monte-Carlo calculations with Fuchs' limiting-sphere theory shows good agreement for the whole size range and highlights the importance of the image force effect for smaller particles. The diffusion-mobility theory of the continuum regime matches the simulation results for the larger particle sizes while differences with Fuchs' limiting-sphere theory in this regime are relatively small. Simulations of non-spherical particles show the power of the code to easily handle more complicated situations. Results of rectangular-shaped and elongated chain-aggregate particles show different charging behaviour compared to theoretical predictions, and indicate the importance of the assumptions for the surface distribution of charges on the particle. In contrast, calculations of 3D cross-shaped aggregate particles, despite having a very irregular geometry, indicate that the spherical shape assumption is reasonable.

1. Introduction

Diffusion charging has become one of the most commonly used methods for charging aerosol particles. Apart from its importance in industrial applications and atmospheric physics, the phenomenon

* Corresponding author. Tel.: +44-1223332681; fax: +44-1223765311.
E-mail address: gb256@eng.cam.ac.uk (G. Biskos).

0021-8502/$ - see front matter © 2003 Elsevier Ltd. All rights reserved.
doi:10.1016/j.jaerosci.2003.11.010

is of significant interest in aerosol-measurement science when electrical mobility analysis is used. The process can be characterised as unipolar or bipolar depending on the polarity of the ions in the gas, and both methods are successfully used in such instruments. However, unipolar diffusion charging proves to be more effective when particles are detected by electrometric methods.

In unipolar diffusion charging, aerosols are allowed to interact with an ionised gas for a certain time, during which randomly moving ions collide with and transfer their charge to the particles. When a particle is charged, the electric field formed in the vicinity induces a repulsive force on the incoming ions reducing the probability of further ion–particle collisions. Absence of any external electric field has to be ensured, although the effect is negligible for particles with diameter less than 1 μm in weak fields (Hinds, 1999; Lawless, 1991).

Both unipolar and bipolar diffusion charging have been studied theoretically and various models that describe the phenomena are available in the literature. Naturally, due to the high complexity of the problem, there is no unique theory for the whole range of particle sizes and different models are often used depending on the relative size of the particles to the ionic mean free path. This, in turn, underlines the importance of the ions in the gas and their associated properties. Several studies conclude that the most abundant ionic species found in positive unipolar aerosol chargers is in the form of hydrated protons with mean free paths ranging from 10 to 20 nm depending on the number of water molecules on the ion (Pui, 1976).

The well-established diffusion-mobility equation is used to predict charging levels for particles in the continuum regime (Arendt & Kallman, 1925; Pauthenier & Moreaut-Hanot, 1932; Fuchs, 1947; Bricard, 1949). For particles in the transition regime, the situation is more complicated and two approaches are commonly used. The first is the limiting-sphere theory (Fuchs, 1963), which can be considered as a correction to the continuum diffusion-mobility equation, while the second is based on approximate solutions of the Boltzmann equation. Using the Knudsen iteration method, several researchers have provided solutions of the BGK Boltzmann approximation equation to estimate ion–particle collision rates (Gentry & Brock, 1967; Gentry, 1972; Marlow & Brock, 1975; Huang, Seinfeld, & Marlow, 1990). Transition regime theories are usually extended to describe diffusion charging in the free molecular regime. However, the controversial model proposed by White (1951), has been extensively used, although its inability to take into account the image force effect can result in significant errors. Models that consider the image force effect have been proposed by later authors (Natanson, 1960; Brock, 1969, 1970).

All the above-mentioned theories describe the evolution of the average charge on particles of a specific size. The stochastic nature of the phenomena was pointed out by Boisdron and Brock (1970), who proposed use of the source-and-sink approach to calculate charge distributions on monodisperse particles. This method, employing combination coefficients from any diffusion charging theory depending on the relative size of the particle to the ionic mean free path, has become common practice.

Several experimental works have been conducted to verify the above-mentioned theories. Liu and Pui (1977), and later Kirsch and Zagnit'ko (1981), presented experimental evidence that support the validity of the diffusion-mobility equation for the continuum regime. Adachi, Kousaka, and Okuyama (1985) found good agreement between their experimental results and Fuchs' limiting-sphere theory for particles in the transition regime. Pui, Fruin, and McMurry (1988), comparing their experimental results with most of the available theories by that time, showed that the limiting-sphere model describes well the phenomenon in the transition regime, while Marlow's approach (Marlow & Brock, 1975) is more appropriate for particles with diameter less than 10 nm at atmospheric

pressure. Adachi, David, and Pui (1992), using a novel design of a unipolar diffusion charger with minimal particle losses showed that the source-and-sink approach, employing combination coefficients determined by the limiting-sphere theory, estimates fractions of charged particles within acceptable error levels.

More complicated phenomena encountered in diffusion charging have been investigated in other works. Marlow (1978a), applying the source-and-sink approach managed to incorporate the existence of several ionic species in the gas. In his next paper, Marlow (1978b) considered aerosol polydispersity and showed that the phenomenon is affected by the particle number density of the gas. Moreover, attempts have been made to determine charging levels for particles of arbitrary shape in a theoretical and experimental way (Laframboise & Chang, 1977; Chang, 1981; Wen, Reischl, & Kasper, 1984a, b; Yu, Wang, & Gentry, 1987; Han, Ranade, & Gentry, 1991; Han & Gentry, 1994).

The analytical theories, however, cannot capture easily aerosol polydispersity and/or particles with complex shapes. In an effort to understand better the diffusion charging process of such particles, a Monte-Carlo code has been developed and is presented in this paper. Monte-Carlo simulations have been used successfully in modelling a wide range of transport phenomena, for example diffusion processes and chemical reactions in the free molecule regime (Bird, 1994), dispersion of solid particles in turbulent flows (Mastorakos, McGuirk, & Taylor, 1990), and particle sintering and coagulation (Akhtar, Lipscomb, & Pratsinis, 1994). Filippov (1993) used the Monte-Carlo approach to investigate the process of diffusion charging of spherical particles in the size range 5–80 nm. His results showed good agreement with the Fuchs' limiting-sphere theory for the transition regime and Brock's model for the free molecular regime.

The power of Monte-Carlo simulations lies in the capability to include the micro-mechanics of the phenomena (ion–molecule collisions, ion and particle motion, etc.), which can then be used over a large number of realisations to compile the average behaviour. The code presented in this paper is capable of simulating aerosol diffusion charging for a wide range of Knudsen numbers and $N_i t$ products. Average number of charges and charge distributions are easily determined by the algorithm for monodisperse aerosols with diameter 5–1000 nm, and $N_i t$ parameters up to 5×10^{12} ions m^{-3} s at atmospheric pressure. Using the ability of the code to simulate non-spherical aerosols, we present some preliminary calculations of arbitrary-shaped particles.

The rest of the paper is organised as follows: in Section 2 we present various theoretical diffusion charging models that are compared later with the Monte-Carlo results, and provide a discussion on the properties of the ions. Section 3 describes the structure of the Monte-Carlo code and highlights the important aspects of the phenomena, while Section 4 presents simulation results and a comparison with the theoretical predictions. Finally, we close with a summary of the most important conclusions.

2. Theoretical background

In this section, we present and discuss various theoretical diffusion charging models that will be tested against the Monte-Carlo simulations. Various concepts and definitions are also introduced followed by a description of the ionic properties which both the theoretical models and the Monte-Carlo code use.

The usual approach for solving the problem of diffusion charging in unipolar ionised gases is based on the source-and-sink theory as proposed by Boisdron and Brock (1970). According to this

method, the evolution of charge distribution on monodisperse particles is given by the solution of an infinite set of differential-difference equations (DDEs) as follows:

$$\frac{dN_{p,0}}{dt} = -\beta_0 N_{p,0} N_i, \tag{1}$$

$$\frac{dN_{p,1}}{dt} = \beta_0 N_{p,0} N_i - \beta_1 N_{p,1} N_i,$$

$$\vdots \tag{2}$$

$$\frac{dN_{p,n}}{dt} = \beta_{n-1} N_{p,n-1} N_i - \beta_n N_{p,n} N_i, \tag{3}$$

where $N_{p,n}$ is the number concentration of particles with n elementary charges, N_i the ion concentration, and β_n the combination coefficient of ions with particles carrying n elementary charges, given by

$$\beta_n = \frac{J}{N_i}. \tag{4}$$

Here $J = dn/dt$ is the flux of ions to the particle estimated by various theories discussed in Sections 2.1 and 2.2. Simultaneous solution of the above system of DDEs provides the average charge and charge distribution on particles of a specific diameter exposed to given $N_i t$ conditions. In practice the number of equations one has to solve is finite, although this has to be high compared to the expected average number of charges.

2.1. Spherical particles

Owing to the high complexity of the problem, there is no unique theory to determine the ionic flux of ions on particles for the whole range of Knudsen numbers, so different models have to be employed depending on the relative size of the particle with the ionic mean free path, λ_i. The following paragraphs give a brief review of the main diffusion charging theories for the different transport regimes. For the rest of the paper a denotes the radius of the particle. However, written as a subscript, a indicates the background gas which for all the results presented is considered to be air at atmospheric pressure.

Continuum regime ($\lambda_i \ll a$): The well-established diffusion-mobility equation is used to describe the process in the continuum regime. In a general formulation, the flux of ions crossing a spherical surfaces of radius r is

$$J(r) = -4\pi r^2 \left(D_i \frac{dN_i}{dr} - Z_i N_i E(r) \right), \tag{5}$$

where D_i and Z_i are the diffusion coefficient and electrical mobility of the ions, respectively, N_i the ion concentration, and E the electric field strength at distance r from the centre of the particle. The solution of Eq. (5) has been given by many authors independently (Arendt & Kallman, 1925; Bricard, 1949; Fuchs, 1947; Pauthenier & Moreaut-Hanot, 1932) and expressed as the ion flux to a

particle of specific size it becomes

$$J = \frac{4\pi D_{\mathrm{i}} N_{\mathrm{i}}}{\int_a^{\infty} (1/r^2) \exp(\phi(r)/kT)\, \mathrm{d}r}. \tag{6}$$

Here k is Boltzmann's constant, T the gas temperature and ϕ the potential at distance r from the centre of the particle. Including the image force the latter is described by

$$\phi(r) = \int_r^{\infty} F\, \mathrm{d}r = K_E \left[\frac{ne^2}{r} - \kappa \frac{a^3}{2r^2(r^2 - a^2)} \right]. \tag{7}$$

In the above equation, F is the ion–particle interaction force, a the particle radius, $\kappa = [(\varepsilon - 1)/(\varepsilon + 1)]e^2$ the image force parameter for particles with dielectric constant ε and $K_E = 1/4\pi\varepsilon_0$ with ε_0 the vacuum permittivity. The first term in the parenthesis corresponds to the Coulomb force while the second term to the image force induced by the ion.

Estimating the integral at the denominator of Eq. (6) can be difficult since the image force at the surface of the particle becomes infinite, and indeed an analytic solution of the continuum regime theory incorporating the image force does not exist. Considering only the Coulomb force one can obtain an analytic solution of the ionic flux to the particle as follows:

$$J = K_E \frac{4\pi D_{\mathrm{i}} N_{\mathrm{i}} ne^2}{akT \left[\exp\left(K_E \frac{ne^2}{akT} \right) - 1 \right]}. \tag{8}$$

It can be easily demonstrated that the effect of the image force diminishes with particle size and becomes negligible for particles greater than a few hundred nm, therefore excluding it from the continuum model is a reasonable assumption. For particles in the transition and free molecular regime, however, the image force is important since the associated potential becomes comparable to the mean thermal energy of the ions.

Transition regime ($\lambda_{\mathrm{i}} \approx a$): As mentioned in Section 1, two widely accepted approaches exist for treating diffusion charging of aerosol particles in the transition regime. The limiting-sphere theory assumes two regions separated by an imaginary sphere concentric to the particle. Between this sphere and the particle surface, motion of the ions is determined by the thermal speed and interaction potential with the particle, while outside the sphere, this is described by the macroscopic diffusion-mobility theory. Fuchs (1963), matching the two fluxes at the surface of the limiting-sphere, derived the following expression for the ion flux to the particle:

$$J = \frac{\pi\gamma \bar{c}_{\mathrm{i}} \delta^2 N_{\mathrm{i}} \exp(-\phi(\delta)/kT)}{1 + \exp(-\phi(\delta)/kT) \frac{\gamma \bar{c}_{\mathrm{i}} \delta^2}{4D_{\mathrm{i}}} \int_{\infty}^{r} (1/r^2) \exp(\phi(r)/kT)\, \mathrm{d}r}, \tag{9}$$

where γ is the probability of an ion entering the limiting-sphere to collide and transfer its charge to the particle, $\bar{c}_{\mathrm{i}}$ the mean thermal speed of the ions, Eq. (20), and δ the limiting-sphere radius given by

$$\delta = \frac{a^3}{\lambda_{\mathrm{i}}^2} \left[\frac{(1 + \lambda_{\mathrm{i}}/a)^5}{5} - \frac{(1 + \lambda_{\mathrm{i}}^2/a^2)(1 + \lambda_{\mathrm{i}}/a)^3}{3} + \frac{2}{15} \left(1 + \frac{\lambda_{\mathrm{i}}^2}{a^2} \right)^{5/2} \right]. \tag{10}$$

In the absence of any electrical forces, the collision probability γ reduces to the square of the ratio of the particle radius over the limiting-sphere radius ($\gamma = a^2/\delta^2$). However, for the case of charged

particles, γ is calculated according to the collision parameter b of the minimum apsoidal distance. Natanson (1960) proposed that this be determined by

$$b^2 = r^2 \left[1 + \frac{2}{3kT}\left[\phi(\delta) - \phi(r)\right]\right]. \tag{11}$$

Setting $\mathrm{d}b^2/\mathrm{d}r = 0$, one can calculate the minimum collision parameter b_m and the associated collision probability as $\gamma = b_{\mathrm{m}}^2/\delta^2$. Hoppel and Frick (1986) provided accurate estimations of collision probabilities for different particle sizes and concluded that, when only attractive encounters are considered, these are not equal to unity as originally stated by Fuchs (1963).

Gentry and Brock (1967) derived an approximate solution of the Boltzmann collision equation by the method of Knudsen iteration. Marlow and Brock (1975), following the same approach and considering Coulomb and image force interaction potentials, showed that the flux of ions to a particle with radius a is

$$J = \frac{\pi a^2 \bar{c}_{\mathrm{i}} N_{\mathrm{i}} E_0}{1 + \lambda E_1 / 2\sqrt{\pi} E_0}, \tag{12}$$

where E_0 and E_1 are the zeroth- and first-order corrections to the free-molecule flux, and $\lambda = a\sqrt{\pi}/\lambda_{\mathrm{i}}((m_a + m_{\mathrm{i}})/m_{\mathrm{i}})$. Their calculations demonstrate that the effect of taking into account the image force term results in significantly higher ion transfer rates for Knudsen numbers greater than one. Huang et al. (1990), pointing out a reduction mistake in this theory, and using the same technique, showed that the ionic flux in the transition and free molecular regime is

$$J = \pi a^2 \bar{c}_{\mathrm{i}} N_{\mathrm{i}} \left(E_0 - \frac{1}{\tau} E_1\right). \tag{13}$$

Here, τ is the relaxation time of the system given by

$$\tau = \frac{D_{\mathrm{i}} + D_{\mathrm{p}}}{a} \sqrt{\frac{m_{\mathrm{i}}}{kT}}. \tag{14}$$

Free molecular regime ($\lambda_{\mathrm{i}} \gg a$): Solution of the diffusion charging problem in the free molecular regime has been based on the kinetic theory of gases, and often the transition regime theories have been successfully extended to describe the problem. White (1951), assuming a Boltzmann spatial distribution of the ions around a charged particle, derived the following expression to predict the mean ionic flux on aerosol particles:

$$J = \pi a^2 \bar{c}_{\mathrm{i}} N_{\mathrm{i}} \exp\left(-K_E \frac{ne^2}{akT}\right). \tag{15}$$

White initially derived and compared the above equation for particles in the continuum regime, but later on it was shown that the model is valid only for the free molecular regime (Liu, Whitby, & Yu, 1967; Gentry & Brock 1967). The integrated form of the above equation is widely used and can be found in many basic textbooks (Willeke & Baron, 1993; Hinds, 1999). However, the drawback of neglecting the image force effect in the above theory was pointed out later by Brock (1969, 1970).

Another early attempt to describe diffusion charging of ultrafine particles, but this time by taking into account the image force effect, was made by Keefe and Nolan (1962). Considering a Maxwellian distribution of ion velocities they derived the ion flux to an uncharged particle as

$$J = \pi a^2 \bar{c}_\mathrm{i} N_\mathrm{i} \left(1 + \sqrt{K_E \frac{\pi e^2}{2akT}} \right). \tag{16}$$

The term in the parenthesis in the above equation is the enhancement factor of the image force. In a later work, Keefe, Nolan, and Scott (1968) presented numerical calculations of combination coefficients of ions with charged particles.

2.2. Non-spherical particles

Diffusion charging theories assuming spherical shaped particles have been widely and successfully used to describe the process. However, several experimental studies that examine arbitrary-shaped particles show significant disagreements when compared with theoretical predictions (Vomela & Whitby, 1967; Kasper & Shaw, 1983), indicating that a more sophisticated analysis is required.

Laframboise and Chang (1977) provided one of the first theoretical models of diffusion charging for non-spherical particles. Based on the diffusion-mobility equation of the continuum regime and obtaining analytical solutions of the electric field around spheroidal charged particles (oblates and prolates), they derived the following equation to calculate the ion flux to non-spherical particles:

$$J = 4\pi N_\mathrm{i} D_\mathrm{i} \frac{L}{\ln(2L)} \frac{\Phi \exp(-\Phi)}{1 - \exp(-\Phi) + Kn_e \Phi}. \tag{17}$$

Here L is the ratio of the polar to the equatorial diameter of the particle ($L \geqslant 1$ for prolate particles), $\Phi = K_E n e^2 \ln(2L)/akTL$ is the dimensionless potential on the surface of the particle, and $Kn_e = 4\pi D_\mathrm{i}/d_\mathrm{p}\bar{c}_\mathrm{i} \ln(2L)$ is the effective Knudsen number.

Chang (1981), in an attempt to provide a simpler and much easier model to use for such particles, derived several approximation equations for the three transport regimes based on Laframboise's theory. For the particular case of prolate particles in the transition regime the approximation model is as follows:

$$\Phi = \begin{cases} 2\left[\sqrt{(1+Kn'_e)^2+(1+Kn'_e)(1+2Kn'_e)K_3\tau}-(1+Kn'_e)\right] \Big/ (1+2Kn'_e) & \text{for } \Phi \leqslant 1, \\ K_3\tau & \text{for } \Phi \leqslant 0.1, \end{cases} \tag{18}$$

where

$$K_3\tau = \frac{e^2}{kT} \frac{N_\mathrm{i} D_\mathrm{i} t}{(1+Kn'_e)\varepsilon_0}, \quad Kn'_e = Kn_e \frac{\cos^{-1}(1/L)}{\ln(L+\sqrt{L^2-1})}$$

for prolate particles. Wen et al. (1984a), following the above-mentioned theories introduced the term of the *charging equivalent diameter* ($d_{qe} = d_\mathrm{p} L/\ln(2L)$) and in a subsequent work (Wen et al., 1984b), approximating the aspect ratio of the particles with the number of elementary particles on chain aggregates, compared Laframboise's theory with experimental results for the case of bipolar charging.

Table 1
Diffusion charging theories compared with the Monte-Carlo simulations

Theory	Reference	Equation	regime	Particle shape	Image force
Diffusion mobility theory	Fuchs (1947)[a]	Eq. (8)	Continuum	Spherical	No
Limiting-sphere theory	Fuchs (1963)	Eq. (9)	Transition	Spherical	Yes
Approx. of Boltzmann's equation	Marlow and Brock (1975)	Eq. (12)	Transition	Spherical	Yes
Approx. of Boltzmann's equation	Huang et al. (1990)	Eq. (13)	Transition	Spherical	Yes
Free molecular regime theory	White (1951)[b]	Eq. (15)	Free molecular	Spherical	No
Non-spherical particle theory	Laframboise and Chang (1977)	Eq. (17)	Continuum	Non-spherical[c]	No
Non-spherical particle theory	Chang (1981)	Eq. (18)	Transition[d]	Non-spherical	No

[a]The theory has been proposed independently by other authors (Arendt & Kallman, 1925; Pauthenier & Moreaut-Hanot 1932; Bricard, 1949).

[b]Although White, 1951 originally derived the equation for the continuum regime, other researchers showed that this is only applicable to the free molecular regime (Liu et al., 1967; Gentry & Brock, 1967).

[c]For prolate and oblate spheroids.

[d]Approximations for the other regimes (continuum and free molecular) are also given by Chang, 1981.

Table 1 gives a descriptive summary of the theories reviewed and compared with the Monte-Carlo in this paper.

2.3. Ion properties

Use of any of the above models to describe diffusion charging requires information on the properties of the ions. There is a substantial amount of literature on mobility measurements for ions produced in atmospheric or laboratory environments. Works ranging from early investigations of ionised gases by Thomson and his group in the Cavendish Laboratory (Thomson, 1896, 1898), to most recent publications (Sakata & Okada, 1994), indicate that ion mobility depends on the chemical composition of the background gas and aging of the ions. It is generally agreed that high mobility ions, once formed, undergo a clustering process resulting in heavier stable ions of lower mobility.

For the particular case of positive ions, the relative humidity of the gas is of high importance because water molecules lead to the formation of hydrated proton clusters (Mohnen, 1977; Kebarle, Searles, Zolla, Scarbrough, & Arshadi, 1967). Many authors have used Langevin's theory (Langevin, 1905) to determine the ionic mass based on mobility measurements. However, the theory is only valid for monoatomic ions and fails for molecular or cluster ions since the effective ionic size and its associated collision cross-section with neutral gas molecules are difficult to predict (Böhringer et al., 1987).

It has been common practice to use experimental data for both of these quantities. Mass and electrical mobility of ions are usually determined by combination of mass spectrometer and drift tube measurements. Kilpatrick (1971) provided one of the most popular experimental data sets on mobilities of ions with masses ranging from 35.5 to 2122 amu. Huertas, Marty, and Fontan (1974) reported similar measurements but specifically for hydrated proton ions, while Meyerott and Reagan (1980), making a review of works on ionic properties, concluded that Kilpatrick's fitted model agrees with most ion-cluster species of mass up to a few thousands amu.

Using experimental indications of the electrical mobility, we can calculate the diffusion coefficient of the ions by the Stokes–Einstein equation

$$D_{\mathrm{i}} = \frac{kTZ_{\mathrm{i}}}{e}, \tag{19}$$

while the mean velocity of the specific ions is given by

$$\bar{c}_{\mathrm{i}} = \sqrt{\frac{8kT}{\pi m_{\mathrm{i}}}} \tag{20}$$

with m_{i} being the mass of the ions.

Once the diffusion coefficient and mean speed of the ions is determined, the mean free path can be calculated according to the theory of binary diffusivity. Huang and Seinfeld (1988) made a brief review on the available models that connect binary diffusivity with the mean free path to conclude that depending on the relative magnitude of the mass of the ions m_{i}, to that of the background gas molecules m_a, one of the following expressions should be used:

$$D_{\mathrm{i}} = \begin{cases} \frac{1}{3}\lambda_{\mathrm{i}}\bar{c}_{\mathrm{i}} & \text{for } m_{\mathrm{i}} \ll m_a, \\ 0.5985\lambda_{\mathrm{i}}\bar{c}_{\mathrm{i}} & \text{for } m_{\mathrm{i}} \approx m_a, \\ \frac{3\pi m_{\mathrm{i}}}{32 m_a}\lambda_{\mathrm{i}}\bar{c}_{\mathrm{i}} & \text{for } m_{\mathrm{i}} \gg m_a. \end{cases} \tag{21}$$

However, most works on aerosol diffusion charging use the Maxwell–Chapman–Enskog theory to determine the mean free path of the ions. According to Pui et al. (1988), this is expressed as

$$D_{\mathrm{i}} = \frac{3}{8}(1+\varepsilon_{\mathrm{i},a})\sqrt{\pi}\lambda_{\mathrm{i}}\left(\frac{m_{\mathrm{i}}+m_a}{m_a m_{\mathrm{i}}}\,kT\right)^{1/2}, \tag{22}$$

where $\varepsilon_{\mathrm{i},a}$ is a correction factor that depends on the relative mass of the two species ($\varepsilon_{\mathrm{i},a}$ ranges from 0.016 to 0.132 for ions and molecules of equal and unequal masses, respectively). Assuming the hydrated proton $H^+(H_2O)_6$, to be the most abundant ionic species with an average mobility $Z_{\mathrm{i}} = 1.4\times10^{-4}\ \mathrm{m^2\ V^{-1}\ s^{-1}}$ (Pui, 1976), mean free paths calculated by Eqs. (21) and (22) are 13.5 and 14.6 nm respectively for $T = 300\ K$.

Another way to determine the ionic mean free path is based on information of the physical size of the ions. Wei and Salahub (1994) determined the geometric structure of the hydrated proton ions by calculating the physical lengths of the bonds. According to their results, H–O bonds in the ion become stronger while the hydrogen bonds become weaker as the number of water molecules on the ion increases. For the particular case of hydrated protons with six water molecules two isomers exist and their physical size, despite the non-spherical shape, is of the order of 1 nm.

In the light of this information, the mean free path of the randomly moving ions can be calculated by simple considerations of the kinetic theory of binary gases (Chapman & Cowling, 1990). According to this theory, the ionic mean free path within the background gas a is

$$\lambda_{\mathrm{i}} = \bar{c}_{\mathrm{i}}\tau_{\mathrm{i},a}, \tag{23}$$

where $\tau_{\mathrm{i},a}$ is the mean time between successive collisions of the ions determined by the following equation:

$$\tau_{\mathrm{i},a} = \frac{N_{\mathrm{i}}}{\nu_{\mathrm{i,i}} + \nu_{\mathrm{i},a}}. \tag{24}$$

Here $v_{\mathrm{i,i}}$ and $v_{\mathrm{i},a}$ are the ion–ion and ion–molecule collision frequencies, respectively:

$$v_{\mathrm{i,i}} = \frac{\sqrt{2}}{2}\pi N_{\mathrm{i}}^2 \sigma_{\mathrm{i,i}}^2 \bar{c}_{\mathrm{i}}, \quad v_{\mathrm{i},a} = \sqrt{2}\pi N_{\mathrm{i}} N_a \sigma_{\mathrm{i},a}^2 \bar{c}_{\mathrm{i},a}. \tag{25}$$

In the above equations $\sigma_{\mathrm{i,i}}$ is the ion collision diameter, $\sigma_{\mathrm{i},a} = \frac{1}{2}(\sigma_{\mathrm{i}} + \sigma_a)$ the binary collision diameter, N_a the background gas concentration and $\bar{c}_{\mathrm{i},a}$ is the relative speed of the ions with the gas molecules:

$$\bar{c}_{\mathrm{i},a} = \sqrt{\frac{4kT}{\pi m_{\mathrm{i},a}}}, \tag{26}$$

where $m_{\mathrm{i},a} = m_{\mathrm{i}} m_a/(m_{\mathrm{i}} + m_a)$ is the reduced mass of the system. Noting that ion concentrations are significantly lower than that of the background gas molecules, the binary collision frequency is much higher compared to the ion–ion collision frequency ($v_{\mathrm{i},a} \gg v_{\mathrm{i,i}}$). Eliminating $v_{\mathrm{i,i}}$ in Eq. (24), and substituting back to Eq. (23) we can write

$$\lambda_{\mathrm{i}} = \frac{\bar{c}_{\mathrm{i}}}{\sqrt{2}\pi N_a \sigma_{\mathrm{i},a}^2 \bar{c}_{\mathrm{i},a}}. \tag{27}$$

Substituting Eqs. (20) and (26) for the mean speeds we can rearrange to obtain

$$\lambda_{\mathrm{i}} = \frac{1}{\pi N_a \sigma_{\mathrm{i},a}^2 \sqrt{1 + m_a/m_{\mathrm{i}}}}. \tag{28}$$

It is obvious that the mean free path of the ions is independent of their concentration and thermal speed. At atmospheric pressure the air molecule concentration is $N_a \approx 2.5 \times 10^{25}\ \mathrm{m}^{-3}$, while the diameter of air molecules is $\sigma_{\mathrm{i}} = 0.25$ nm. Using Eq. (28), calculations based on the hydrated proton size ($\sigma_{\mathrm{i}} \approx 1$ nm) as estimated by Wei and Salahub (1994), corroborate that the ionic mean free path is of the order of 15 nm.

To summarise, ionic species of unipolar ions found in aerosol chargers are dynamically changing species growing by a series of clustering reactions that depend on the composition of the gas. Owing to this dynamic change, such gases consist of several kinds of ions that vary in electrical mobility. In order to keep analysis of such systems simple it is a common practice to assume a single species with representative properties. For the particular case of the present Monte-Carlo simulations, this assumption, apart from simplifying the algorithm, it significantly reduces the required computational power. All calculations presented in the following sections assume a mean free path of the ions of 14.5 nm.

3. The Monte-Carlo simulation

The basic concept of the Monte-Carlo algorithm is presented in Fig. 1. The simulation volume consists of a system of uniformly distributed particles and ions that move randomly according to their thermal velocities. Particles, being significantly more massive compared to ions, have much smaller thermal speeds; thus, considering fixed particle positions in the simulation volume is a reasonable assumption that saves computational power. The error of this assumption is inversely proportional to particle size. However, even for the smallest particles investigated in this work (i.e. $d_{\mathrm{p}} = 5$ nm), the mean speed is one order of magnitude lower compared to that of the ions if we assume a typical particle density of 2 g cm^{-3}. All the results presented in this work regard particles fixed within the

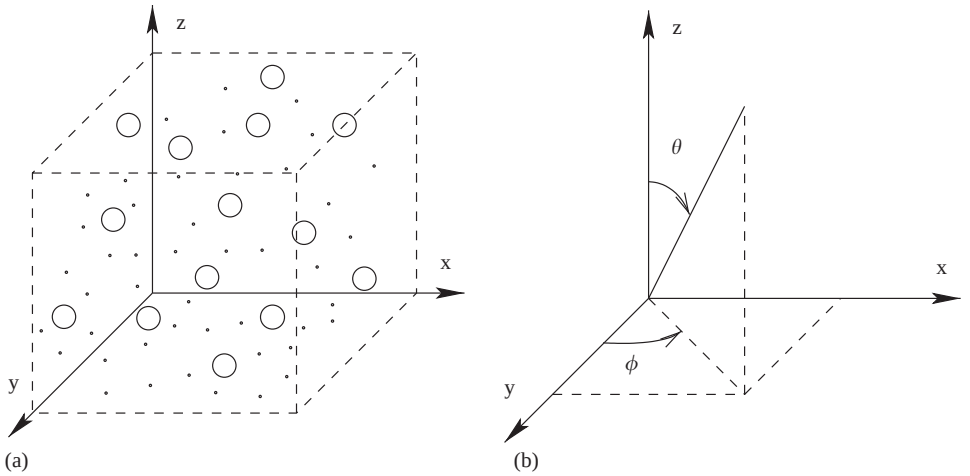

Fig. 1. Schematic representation of the Monte-Carlo simulation code. (a) Monte-Carlo simulation volume, and (b) Ion particle system.

simulation space, although the effect of their random thermal motion can be investigated at the cost of computational time.

Having the positions of the particles fixed in the simulation volume, great amount of computational power is spent to describe the random motion of the ions in the gas. This motion is fully described by the thermal speed and mean free path of the ions. As mentioned in the previous section, ion concentrations in unipolar environments is sufficiently low that ion–ion collisions can be neglected. For this reason, we can assume that the velocity distribution of the ions is completely determined by ion–neutral molecule interactions. Therefore, far away from charged particles (i.e. in the absence of any external force), the ions move in straight paths between collisions. The algorithm uses a simulation time step Δt equal to the mean time between successive ion–neutral molecule collisions calculated by Eq. (24). At the beginning of every time step, an ion–molecule collision occurs resulting in a new random velocity of the ion. A pseudo-random number generator produces Maxwellian thermal velocities for the ions at every time step. Ascribing new velocities at the beginning, and calculating the new positions at the end of every time step, random-walk paths of the ions are followed throughout the simulation.

When an ion is close to a charged particle, its velocity is significantly altered by the ion–particle interaction force, and the associated speed distribution departs from Maxwellian. The path of the ion in this case is calculated by solving the equation of motion for the duration of Δt. In the vicinity of a charged particle this becomes

$$m_{\mathrm{i}} \frac{\mathrm{d}\mathbf{v}_{\mathrm{i}}}{\mathrm{d}t} = q\mathbf{E}, \tag{29}$$

where $\mathbf{E} = -\nabla\phi(r)$ is the electric field induced by the charged particle. Solving the above equation numerically along the ionic free flight results in the calculation of the ion trajectories close to a charged particle. Despite the curved trajectories of the ions now, their mean free path change is assumed to be insignificant, allowing for a collision with a neutral molecules at the end of every time step. A new random velocity is ascribed to the ion and its new path calculated according to Eq. (29).

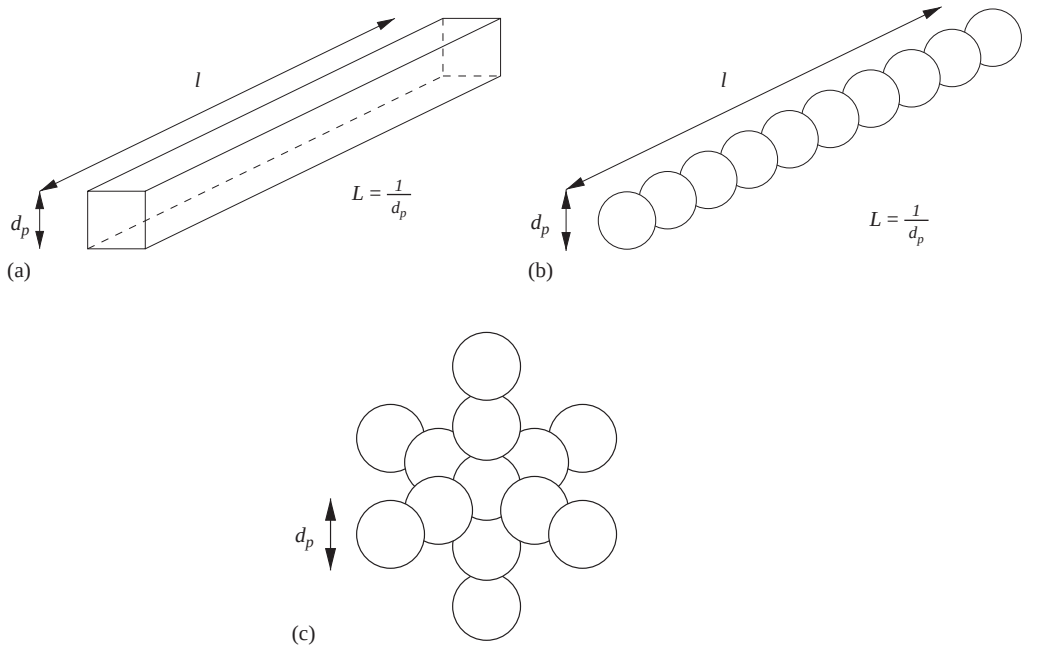

Fig. 2. Schematic layout of non-spherical particles investigated with the Monte-Carlo simulation code. (a) Rectangular-shape particle, (b) Chain aggregate, and (c) 3D Cross-shape aggregate.

Although solution of the equation of motion fully describes the ionic trajectories close to a charged particle, one important point regarding calculations of the repulsive forces (in other words, the electric field **E**) was raised by some preliminary simulations of non-spherical particles. All charging theories considering spherical particles assume that the total charge is located at the centre of the particle, and the induced forces are calculated accordingly. However, ionic flux variations can be expected when the location of the charge is acentric, or in more complicated cases, when the elementary charges are distributed on the surface of the particle. Information of the charge distribution on the particle can be difficult to obtain, and two extreme cases can be distinguished: (a) the total charge is located at the centre of the particle and (b) every elementary charge is located at the point on the surface of the particle where an ion has collided.

It is obvious that the latter case results in much more complicated analysis, and in case one wants to simulate the phenomena using Monte-Carlo techniques, the computational power required will be large. In order to overcome this problem, we considered that every particle consists of smaller elementary spherules. This in fact is a very realistic situation since aggregates are very common particles. Ion trajectories are then determined based on the total induced force on the ion, calculated from the centres of every elementary particle. At the end of the simulation, the total number of charges on the particle is the sum of the charges on every elementary particle. Two different kinds of aggregates where the elementary particles were arranged in a simple line-chain and 3D cross-shape configurations were investigated. Simulations of rectangular-shaped particles were also performed to compare their charging behaviour with spherical and aggregate particles. Fig. 2 shows a diagram of the three types of non-spherical particles investigated in this paper.

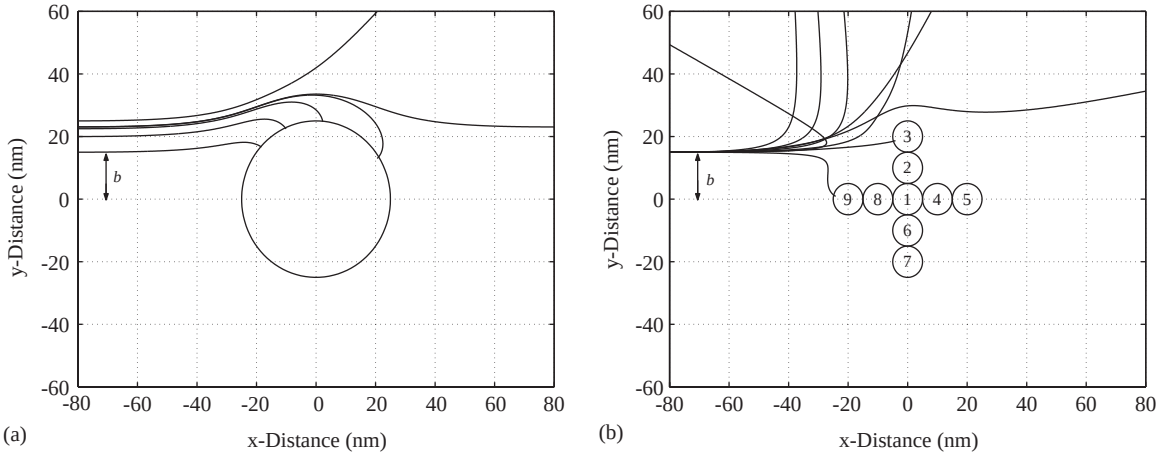

Fig. 3. Ion trajectories in the vicinity of singly charged spherical particles and aggregates. (a) Spherical particle, and (b) Cross-shape aggregate.

Assuming no background gas, Fig. 3 shows 2D projections of calculated ion trajectories close to 50 nm spherical and aggregate particles with one elementary charge. Comparing these trajectories, we can see that ion-particle collision probabilities, apart from being a function of the collision parameter b, also depend on the location of the charge on the particle, or to be more precise, on which elementary particles carry charges.

The induced repulsive force on ions close to a charged spherical particle lies along the line that passes through the centres of the two species (ions and particles) as demonstrated in Fig. 1b. Considering that this has to be calculated and converted into rectangular coordinates for all the time steps of integration of Eq. (29), it is obvious that these sub-calculations can take much of the computational power. For computational efficiency, a sphere is defined around the particle equal to few times its size. When an ion is within this sphere the sub-routine that solves Eq. (29) is used. Outside this region, motion of particles is described by the random thermal velocity only.

The ion concentration is kept constant throughout the simulations by assuming periodic boundary conditions (i.e. once an ion exits the simulation volume from one boundary, a new one enters from the opposite boundary in the following time step). Moreover, when an ion is attached to a particle, a new ion enters the simulation volume in a random manner from the boundaries. Summarising all the individual steps described in this section, Fig. 4 shows the flow chart of the Monte-Carlo code.

The simulations involve statistical error. This error is inversely proportional to the square root of the number of independent observations, or in terms of the present model, from the number of simulated particles. Hence, the error in the mean number of elementary charges collected by the particles is

$$\text{Error} = \frac{\sigma}{\sqrt{N_\text{p}}}. \tag{30}$$

Here σ is the standard deviation of the charge distribution. Depending on the required accuracy and the available computational power, the simulation box length can vary from few tens to few

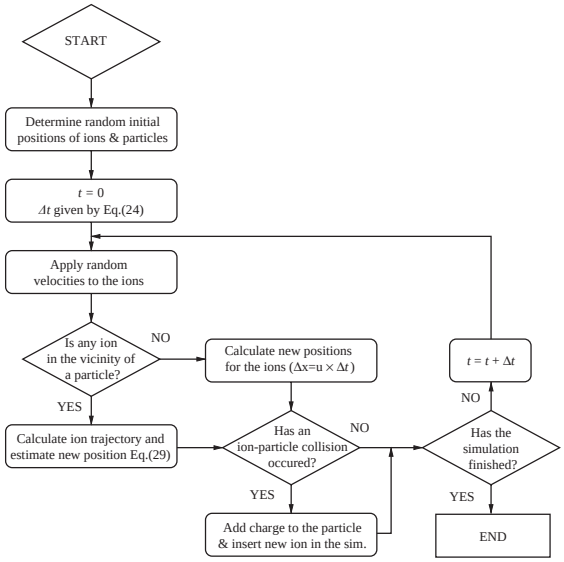

Fig. 4. Flow chart of the Monte-Carlo simulation code.

hundreds of μm. Results presented in this paper required simulation times of the order of weeks on a modern 2 GHz IBM-PC compatible computer for typical systems of 1000 particles.

4. Results and discussion

This section presents the results of the Monte-Carlo simulations. Calculations for spherical aerosols and comparison with theoretical models are given first, followed by simulations of non-spherical particles that include rectangular elongated and aggregate shapes. All the theoretical models used to compare with the Monte-Carlo results were produced by numerical solution of the source-and-sink method using the different ion-flux equations as described in Section 2.

4.1. Spherical particles

The output of the simulations is given in a particle-charge versus time format. Fig. 5 shows the evolution of average charge for different monodisperse aerosols when the image force effect is taken into account. It is evident that calculations for larger particles agree better with the continuum model, while those of smaller particles with the limiting-sphere theory. The increasing pattern of the average charge is similar for all particle sizes, and in most cases agreement with the theoretical models is achieved to within 1%. This good agreement with the widely accepted theories of the continuum and transition regime builds confidence for the present Monte-Carlo method.

Fig. 6 presents in more detail the evolution of different particle species (characterised according to the number of charges they carry). Taking all the particles to be uncharged at the beginning of the simulation, concentrations of particles carrying $1, 2, \ldots, n$ elementary charges are calculated.

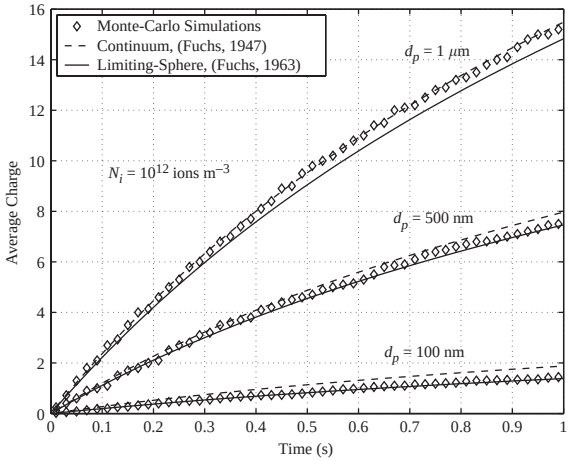

Fig. 5. Evolution of the average number of charges on monodisperse spherical particles.

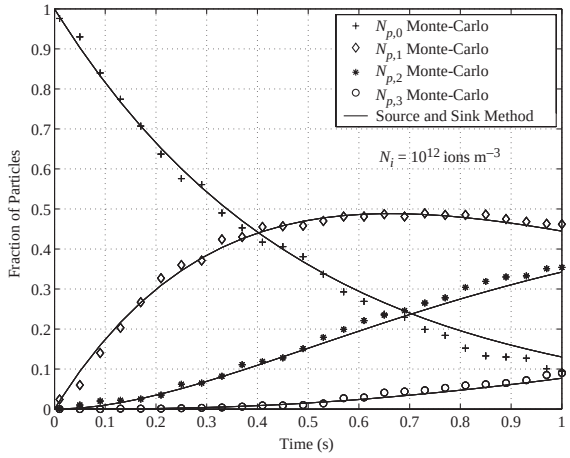

Fig. 6. Evolution of charged particle species on monodisperse particles with diameter $d_p = 100$ nm.

The calculations shown in this figure are for 100 nm spherical particles and an interaction potential that takes into account the image force effect. It is clear that the Monte-Carlo simulations agree well with the source-and-sink approach, if the limiting-sphere theory is used to estimate combination coefficients.

Figs. 7 and 8 show the average charge as a function of particle size with and without taking into account the image force effect, respectively. It is evident that White's theory under-predicts charging levels for particles in the free molecular and transition regimes where the image force parameter is significant. For particles with diameter greater than 200 nm, White's theory over-predicts average charge by as much as a factor of two. The crossing point of the Monte-Carlo data and White's theory, however, can be different depending on the $N_i t$ product.

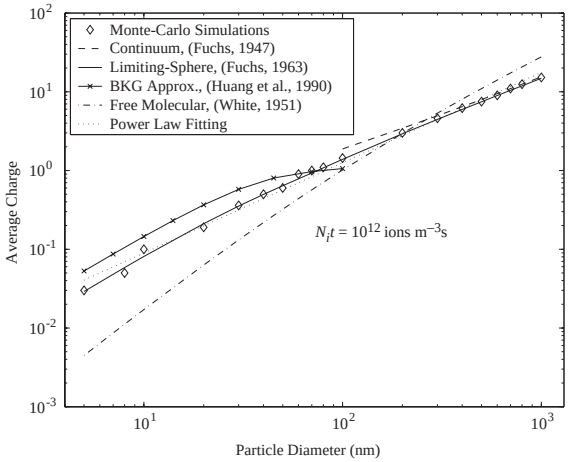

Fig. 7. Average charge of spherical particles as a function of size (with image force consideration).

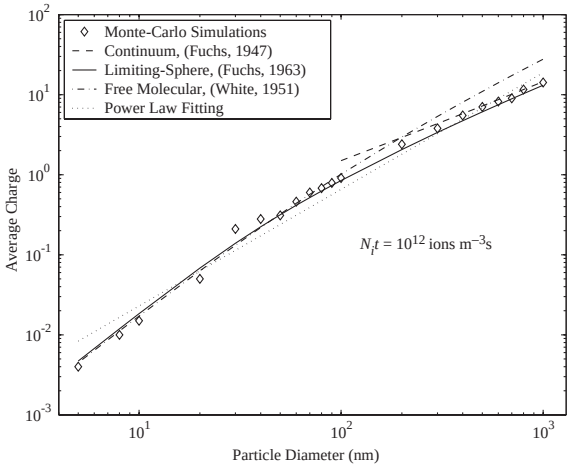

Fig. 8. Average charge of spherical particles as a function of size (without image force consideration).

When the image force effect is ignored, the limiting-sphere theory matches White's equation for the smaller particle sizes. For the particular simulations shown in Figs. 7 and 8, the effect of the image force appears to be significant for particles less than 100 nm, while for particles in the continuum regime it is negligible. Simulation results agree with the limiting-sphere theory for the whole range of particles investigated in this work. Agreement of the results with the continuum theory is better for particles with diameter greater than 500 nm, although due to the logarithmic scale of the graphs this is not so obvious.

Using diffusion charging models based on Boltzmann approximation techniques, specifically Eq. (13), seems to over-predict average charges for particles in the transition regime. The difference between simulations and this model lies in the Brownian motion of the particles which is

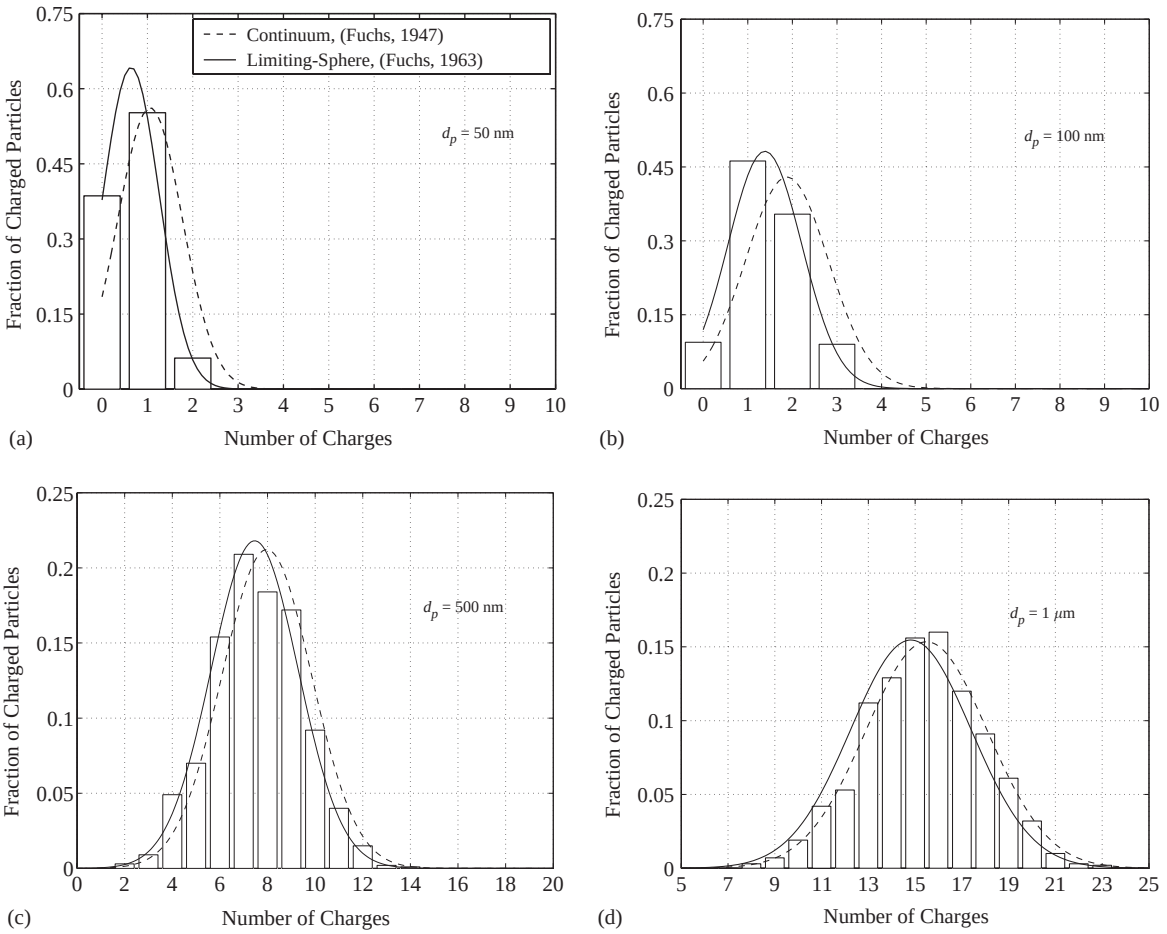

Fig. 9. Charge distributions on monodisperse spherical particles at $N_i t = 10^{12}$ ions m^{-3} s.

not considered by the code at present. Keeping in mind that all the simulations refer to non-moving particles while Eq. (13) takes into consideration both ion and particle diffusivities, differences, as expected, are higher for the smaller particles whose Brownian motion is more intense.

Fitting a power-law model to the Monte-Carlo data, we observe that the slope of the curve is different depending on whether the image force effect is included in the calculations or not. Considering only Coulomb interaction potentials, a power law of the order of 1.1 fits the data, while for interaction potentials determined by Eq. (7), the estimated slope is equal to 1.3 when $\kappa = e^2$. Slightly different slopes are predicted for other $N_i t$ products.

Apart from the average charge on monodisperse particles, information on the charge distribution is equally important when diffusion charging is used in particle spectrometers prior to classification. As Fig. 9 shows, the Monte-Carlo code and the source-and-sink theory indicate that the number of charges on monodisperse particles follow a Gaussian distribution. Combination coefficients used for the theoretical calculations in this figure are estimated by the continuum and limiting-sphere models.

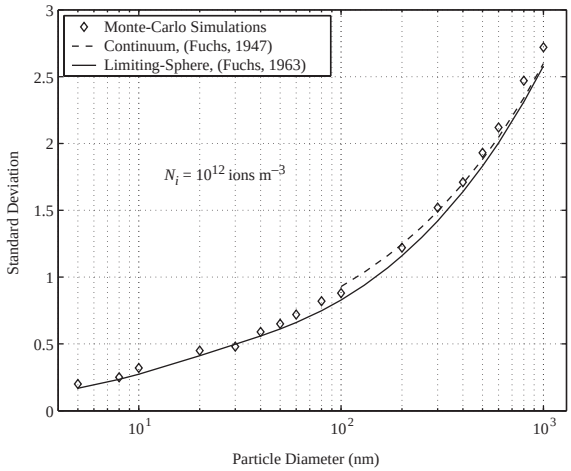

Fig. 10. Standard deviation of charge distribution on monodisperse particles as a function of their size.

It is obvious that simulations of large particles agree better with the former and results of the small particles with the latter. Fig. 10 shows that the standard deviations of charge distributions increases with particle size indicating wider charge and mobility distributions. This is captured by both the source-and-sink theory and the Monte-Carlo calculations.

In summary, average number of charges on spherical particles predicted by the Monte-Carlo simulations show good agreement with predictions of the diffusion-mobility and limiting-sphere theories for the continuum and transition regime, respectively. The importance of the image force effect for the smaller particles is demonstrated by comparing the results with White's equation. The results indicate a change in the slope of the average-charge versus particle-diameter curve depending on the image force consideration. Finally, the simulations show that charge on monodisperse particles follows Gaussian distributions, as also predicted by the source-and-sink approach.

4.2. Non-spherical particles

In an attempt to investigate the effect of particle shape, some initial simulations were performed for rectangular-shaped and aggregate particles. Fig. 11 shows simulations of three different rectangular-shaped particles with aspect ratios 1 (square particle), 5 and 10. In order to make these particles comparable, their dimensions were such that the total surface of all three particles was approximately the same. Image forces are not included in those calculations due to the shape and size of the particles (note that image force potential is comparable to the mean ion thermal energy at distances similar to their mean free path).

Despite the fact that all three particles have equal surface area, charging behaviour appears to be quite different. In fact, the mean number of charges the aggregates acquire appears to be a stronger function of the aspect ratio rather than the physical size of the particles. The results, however, raise the question of whether assuming a uniform potential according to Coulomb's law calculated from the metacentre of the charged particle is realistic. Indeed, motion of ions near the corners of the rectangular particles is dominated by their thermal speed, while ions near the metacentre

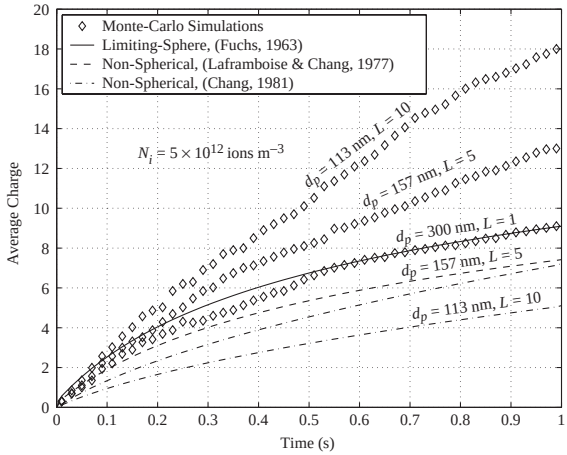

Fig. 11. Average charge of rectangular-shape elongated particles in comparison with theoretical predictions of spherical and non-spherical particles.

of the particle (where the particle charge is located) are retarded by the repulsive electric field. Therefore, dependence of ion flux on the charging state of the particle decreases as the aspect ratio increases.

Comparing results of spherical with square particles of the same size one can see the different charging pattern. For the 300 nm particle, the charging slope (in other words the ionic flux), is slightly higher compared to the 340 nm spherical particle. For elongated particles the discrepancy is higher when compared to non-spherical theories and can be attributed to the difference in calculating the interaction potential as shown in Fig. 11. Mean numbers of charges calculated by the non-spherical particle theories are actually reduced compared to the charged particle, indicating an opposite behaviour compared to the Monte-Carlo simulations. Predictions made with Laframboise's theory (Laframboise & Chang, 1977) indicated that charging behaviour of the two elongated particles are very similar while Chang's theory (Chang, 1981) shows mean charge to be inversely proportional with aspect ratio.

To investigate a more realistic situation, chain aggregate particles were simulated with the Monte-Carlo code. Ten elementary spherical particles of 50 nm diameter were placed along a straight line to form a 500 nm long aggregate (Fig. 2b). Assuming that the particles are electrically isolated from each other, interaction potentials of the ion-aggregate system were determined based on the total force on the ion (sum of forces induced by every elementary particle). Simulations performed for this type of particles included consideration of the image force.

Fig. 12 shows the charging behaviour of such chain aggregates in comparison with a rectangular-shape elongated particles of similar dimensions (50 nm width and 500 nm length). The total number of elementary charges on the chain aggregates appears to be approximately 10% lower compared to the rectangular-shaped particles. Such behaviour is expected since the elementary charges are now better distributed along the particle, and the effect of the repulsive electrostatic force can be equally important at any point. However, in an elementary particle basis, the mean number of charges is significantly reduced compared to the case where 50 nm monodisperse particles are uniformly

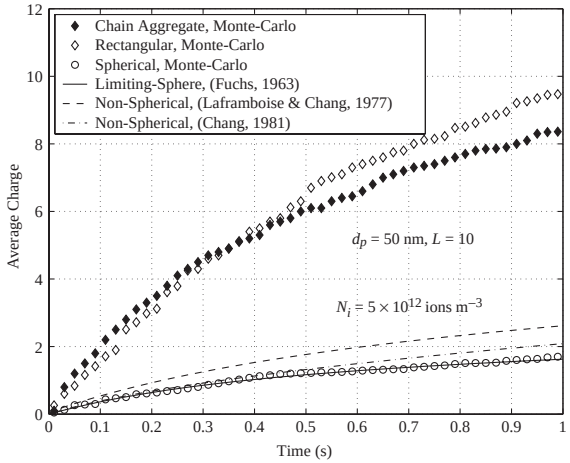

Fig. 12. Average charge of chain aggregates in comparison with rectangular-shape elongated and spherical particles.

distributed in space. Monte-Carlo simulations and theoretical predictions of 50 nm spherical particles are also included in the figure.

The Monte-Carlo results show significant differences from the charging theories of non-spherical particles. Both theories predict mean charges on the aggregate that are 65–75% lower compared with the Monte-Carlo simulations. It should be mentioned, however, that Laframboise's theory (Laframboise & Chang, 1977) is applicable to the continuum regime, and only Chang's approximation (Chang, 1981) for the transition regime can be thought as comparable with the results presented in Fig. 12. This comparison highlights the difference in the distribution of the electric field around a non-spherical charged particle. Theoretical models assume a uniform potential around the particle by taking into account their aspect ratio and calculating the forces from the centre of the spheroids. On the other hand, the Monte-Carlo algorithm determines the electric field around the aggregates as the superposition of fields induced by the individual elementary particles, and therefore its characteristic is a function of the charge distribution on the aggregate. This difference can be partly attributed to the limitation of the non-spherical particle theories to take into account the image force effect. However, the image force effect compared to the surface distribution difference is believed to be less important.

Simulations of elongated rectangular-shaped and chain aggregate particles highlight the effect of surface charge distribution on their charging behaviour. Taking that into account and considering that geometry of real-life agglomerate particles have a more arbitrary configuration, we performed some preliminary calculations of slightly more complicated aggregates. To form these agglomerates, elementary spherical particles of 10 nm diameter were placed in a 3D cross-shape configuration. Using 13 elementary particles an agglomerate of 50 nm effective length was formed (Fig. 2c).

Fig. 13 presents simulations of the average charge evolution on these 3D cross-shape aggregate particles. The results are compared with theoretical predictions for spherical and non-spherical particles as well as with Monte-Carlo simulations of spherical particles of the size of the aggregate (50 nm). Charging behaviour of 3D cross-shaped aggregates seem very similar to those of spherical particles of the same size, while the limiting-sphere theory assuming spherical shapes appears to

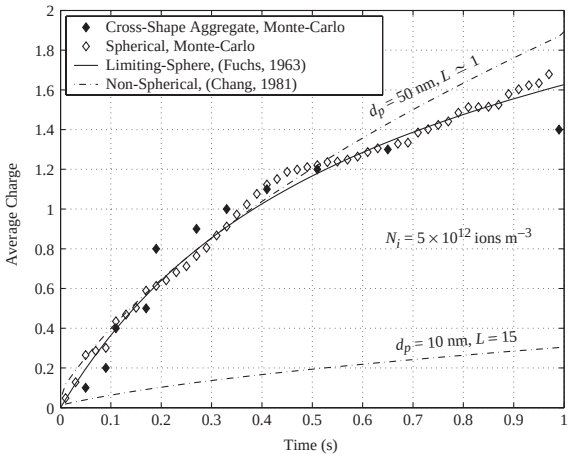

Fig. 13. Average charge of 3D cross-shape aggregates in comparison with Monte-Carlo simulations of spherical particles and theoretical predictions of spherical and non-spherical particles.

interpret both cases well. Agreement with the non-spherical particle theory on the other hand is very poor, and calculations seem to under-predict charging levels of such aggregates even at extreme assumptions of their aspect ratio. Using the same theory but for a primary particle diameter of 50 nm with an aspect ration close to unity gives better agreement with the Monte-Carlo calculations.

These results indicate that depending on the configuration of the aggregate particles, the spherical shape assumption can be reasonable to use with existing diffusion charging theories. However, one should keep in mind that the most probable number of elementary charges on 50 nm particles would be one as shown in Fig. 9, making the effect of the electrostatic repulsion less significant. Also, it should be pointed out that due to the high complication of geometry definition of the aggregate particles, simulations were only feasible for a system of 10 particles within the simulation volume. The associated statistical error of such a system is of the order of 20% for aerosols of this size.

To summarise, simulations of rectangular-shape and elongated chain-agglomerate particles appeared to have different charging behaviour compared to theoretical predictions. This increasing difference with aspect ratio of the particles shows the importance of the assumption of the surface charge distribution, and whether considering all the charge to be located at the metacentre of the aggregates is meaningful. Simulations of 3D cross-shape aggregate particles on the other hand, indicate that the spherical shape assumption is reasonable.

5. Conclusions

In this paper, we used the Monte-Carlo approach to determine charging levels of spherical and non-spherical particles exposed to unipolar ions. The algorithm simulates random motion of ions in aerosol gases, and allows for the calculation of the average charge and charge distribution on particles for a wide range of Knudsen numbers.

Results were presented for monodisperse aerosols in the size range 5–1000 nm and $N_i t$ products of up to 5×10^{12} ions m^{-3} s. For spherical particles comparison of the results with the diffusion-mobility

equation of the continuum regime shows agreement only for the larger particles, while the limiting-sphere theory matches the simulations for the whole size range. The calculations highlight the importance of the image force effect, especially for the smaller particle sizes, and predict different slopes of the average-charge versus particle-diameter curves depending on the consideration of the image force effect.

Simulations for non-spherical particles show the power of the method to provide a better understanding of diffusion charging phenomena. The simulations indicate that the behaviour of rectangular-shaped particles is strongly dependent on their aspect ratio. Charging behaviour of such particles showed significant differences when compared with theoretical predictions. Chain aggregates also showed a different behaviour when compared with analytical theories of elongated spheroids, whereas charging of 3D cross-shape aggregates showed reasonably good agreement with theories assuming spherical particle shapes.

The results of non-spherical particles indicate that shape is an important parameter for diffusion charging, and although some theories are available to describe the phenomena, the Monte-Carlo approach can provide a useful tool for studying such processes further. The Monte-Carlo algorithm presented in this paper can be easily extended to investigate additional phenomena encountered in aerosol diffusion chargers (i.e. the effect of external electric field, initial charge on the particles, different ion–particle interaction potentials, Brownian motion of particles, etc.). The method can also handle bipolar diffusion charging, and its power can be used to consider situations like particle polydispersity or ions with a range of mobilities that are difficult to treat theoretically.

References

Adachi, M., David, F. J., & Pui, D. Y. H. (1992). High-efficiency unipolar aerosol charger using a radioactive alpha source. *Journal of Aerosol Science*, *23*, 123–137.

Adachi, M., Kousaka, Y., & Okuyama, K. (1985). Unipolar and bipolar diffusion charging of ultrafine aerosol particles. *Journal of Aerosol Science*, *16*, 109–123.

Akhtar, M. K., Lipscomb, G. G., & Pratsinis, S. E. (1994). Monte Carlo simulation of particle coagulation and sintering. *Aerosol Science and Technology*, *21*, 83–93.

Arendt, P., & Kallman, H. (1925). The mechanism of charging of mist particles. *Zeitshrift fur Physik*, *35*, 421–441 (in German).

Bird, G. A. (1994). *Molecular gas dynamics and the direct simulation of gas flows*. Oxford: Oxford University Press.

Böhringer, H., Fehey, D. W., Lindinger, W., Howorka, F., Fehsenfeld, F. C., & Albritton, D. L. (1987). Mobilities of several mass-identified positive and negative ions in air. *International Journal of Mass Spectrometry and Ion Processes*, *81*, 46–65.

Boisdron, K., & Brock, J. R. (1970). On the stochastic nature of the acquisition of electrical charge and radioactivity by aerosol particles. *Atmospheric Environment*, *4*, 35–50.

Bricard, J. (1949). L' equilibre ionique de la basse atmosphere. *Journal of Geophysical Research*, *54*, 39–52 (in French).

Brock, J. R. (1969). Aerosol charging: The role of image force. *Journal of Applied Physics*, *41*, 843–844.

Brock, J. R. (1970). Unipolar diffusion charging of aerosols and the image force. *Journal of Colloid and Interface Science*, *33*, 473–474.

Chang, J.-S. (1981). Theory of diffusion charging of arbitrary shaped conductive aerosol particles by unipolar ions. *Journal of Aerosol Science*, *12*, 19–26.

Chapman, S., & Cowling, T. G. (1990). *The mathematical theory of non-uniform gases*. Cambridge, MA: Cambridge University Press.

Filippov, A. V. (1993). Charging of aerosols in the transition regime. *Journal of Aerosol Science*, *24*, 423–436.

Fuchs, N. A. (1947). On the charging of particles in atmospheric aerosols. *Izvestiia Akademii Nauk SSSR. Seriia Geograficheskaia i Geofizicheskaia*, *11*, 341–348 (in Russian).

Fuchs, N. A. (1963). On the stationary charge distribution on aerosol particles in a bipolar ionic atmosphere. *Geofisica Pura e Applicata*, *56*, 185–193.

Gentry, J. W. (1972). Charging of aerosol by unipolar diffusion of ions. *Journal of Aerosol Science*, *3*, 65–76.

Gentry, J. W., & Brock, J. R. (1967). Unipolar diffusion charging of small aerosol particles. *Journal of Chemical Physics*, *47*, 64–69.

Han, R. J., & Gentry, J. W. (1994). Evolution of charge distributions of non-spherical particles undergoing unipolar charging. *Journal of Aerosol Science*, *25*, 499–508.

Han, R. J., Ranade, M. B., & Gentry, J. W. (1991). Rate of unipolar charging of ultrafine thin platelets. *Aerosol Science and Technology*, *15*, 184–190.

Hinds, W. C. (1999). *Aerosol technology: Properties, behavior, and measurement of airborne particles* (2nd ed). New York: Wiley.

Hoppel, W. A., & Frick, G. M. (1986). Ion-aerosol attachment coefficients and the steady-state charge distribution on aerosols in a bipolar ion environment. *Aerosol Science and Technology*, *5*, 1–21.

Huang, D. D., & Seinfeld, J. H. (1988). On the relation between binary diffusivity and mean free path. *Journal of Colloid and Interface Science*, *125*, 733–735.

Huang, D. D., Seinfeld, J. H., & Marlow, W. H. (1990). BKG equation solution of coagulation for large Knudsen number aerosols with a singular attractive contact potential. *Journal of Colloid and Interface Science*, *140*, 258–276.

Huertas, M. L., Marty, A. M., & Fontan, J. (1974). On the nature of positive ions of tropospheric interest and on the effect of polluting organic vapors. *Journal of Geophysical Research*, *79*, 1737–1743.

Kasper, G., & Shaw, D. T. (1983). Comparison size distribution measurements on chain aggregates. *Aerosol Science and Technology*, *2*, 369–381.

Kebarle, P., Searles, S. K., Zolla, A., Scarbrough, J., & Arshadi, M. (1967). The solvation of hydrogen ion by water molecules in the gas phase. Heats and entropies of solvation of individual reactions. *Journal of the American Chemical Society*, *89*, 6393–6399.

Keefe, D., & Nolan, P. J. (1962). Combination coefficients of ions and nuclei. *Proceedings of the Royal Irish Academy*, *62*, 43–53.

Keefe, D., Nolan, P. J., & Scott, J. A. (1968). Influence of coulomb and image forces on combination in aerosols. *Proceedings of the Royal Irish Academy*, *66*, 17–29.

Kilpatrick, W. D. (1971). An experimental mass-mobility relation for ion in air at atmpospherical pressure. *Pages 320–327 of*: *19th Annual Conference on Mass Spectrometry and Allied Topics*.

Kirsch, A. A., & Zagnit'ko, A. V. (1981). Diffusion charging of submicrometer aerosol particles by unipolar ions. *Journal of Colloid and Interface Science*, *80*, 111–117.

Laframboise, J. G., & Chang, J.-S. (1977). Theory of charge deposition on charged aerosol particles of arbitrary shape. *Journal of Aerosol Science*, *8*, 331–338.

Langevin, M. P. (1905). Une formule fondamentale de théorie cinétique. *Annales de Chimie et de Physique*, *5*, 245–288 (in French).

Lawless, P. A. (1991). Particle charging bounds, symmetry relations, and an analytic charging rate model for the continuum regime. *Journal of Aerosol Science*, *27*, 191–215.

Liu, B. Y. H., & Pui, D. Y. H. (1977). On unipolar diffusion charging of aerosols in the continuum regime. *Journal of Colloid and Interface Science*, *58*, 142–149.

Liu, B. Y. H., Whitby, K. T., & Yu, H. S. (1967). On the theory of charging of aerosol particles by unipolar ions in the absence of an applied electric field. *Journal of Colloid and Interface Science*, *23*, 367–378.

Marlow, W. H. (1978a). Unipolar aerosol diffusion charging I. Particle dielectric and ion mobility distribution effects. *Journal of Colloid and Interface Science*, *64*, 543–548.

Marlow, W. H. (1978b). Unipolar aerosol diffusion charging II. Ion and aerosol polydisepersities: The 'diffusion charging mobility analysis' hypothesis. *Journal of Colloid and Interface Science*, *64*, 549–554.

Marlow, W. H., & Brock, J. R. (1975). Unipolar charging of small aerosol particles. *Journal of Colloid and Interface Science*, *50*(1), 32–38.

Mastorakos, E., McGuirk, J. J., & Taylor, A. M. K. P. (1990). The origin of turbulence acquired by heavy particles in a round turbulent jet. *Particle and Particle Systems Characterisation*, *7*, 203–208.

Meyerott, R. E., & Reagan, J. B. (1980). The mobility and concentration of ions and the ionic conductivity in the lower stratosphere. *Journal of Geophysical Research*, *85*, 1273–1278.

Mohnen, V. A. (1977). Formation, nature and mobility of ions of atmospheric importance. In *Electrical Processes in Atmospheres*, edited by Dolezalek, H. and Reiter, R., Dr. Dietrich Steinkopff Verlag, Darmstadt, Germany, pp. 1–17.

Natanson, G. L. (1960). On the theory of the charging of a microscopic aerosol particles as a result of capture of gas ions. *Soviet Physics Technical Physics*, *5*, 538–551.

Pauthenier, M. M., & Moreaut-Hanot, M. M. (1932). Le charge des particules sphériques dans un champ ionisé. *Journal de Physique*, *7*(3), 591–613 (in French).

Pui, D. Y. H. (1976). *Experimental study of diffusion charging*. Ph.D. Thesis, University of Minnesota, Department of Mechanical Engineering.

Pui, D. Y. H., Fruin, S., & McMurry, P. H. (1988). Unipolar diffusion charging of ultrafine aerosols. *Aerosol Science and Technology*, *8*, 173–187.

Sakata, S., & Okada, T. (1994). Effect of humidity on hydrated cluster-ion formation in a clean room corona discharge neutralizer. *Journal of Aerosol Science*, *25*, 879–893.

Thomson, J. J. (1896). On the passage of electricity through gases exposed to Röntgen rays. *Philosophical Magazine*, *42*, 392–407.

Thomson, J. J. (1898). On the charge of electricity carried by the ions produced by Röntgen rays. *Philosophical Magazine*, *46*, 528–545.

Vomela, R. A., & Whitby, K. T. (1967). The charging and mobility of chain aggregate smoke particles. *Journal of Colloid and Interface Science*, *25*, 568–576.

Wei, D., & Salahub, D. R. (1994). Hydrated proton clusters and solvent effects on the proton transfer barrier: A density function study. *Journal of Chemical Physics*, *101*, 7633–7642.

Wen, H. Y., Reischl, G. P., & Kasper, G. (1984a). Bipolar diffusion charging of fibrous aerosol particles I. Charging theory. *Journal of Aerosol Science*, *15*, 89–101.

Wen, H. Y., Reischl, G. P., & Kasper, G. (1984b). Bipolar diffusion charging of fibrous aerosol particles II. Charge and electrical mobility measurements on linear chain aggregates. *Journal of Aerosol Science*, *15*, 103–122.

White, H. J. (1951). Particle charging in electrostatic precipitation. *AIEE Transactions*, *70*, 1186–1191.

Willeke, K., & Baron, P. A. (1993). *Aerosol measurement: Principles, techniques, and applications*. New York: Wiley.

Yu, P. Y., Wang, C. C., & Gentry, J. W. (1987). Experimental measurement of the rate of unipolar charging of actinolite fibers. *Journal of Aerosol Science*, *18*, 73–85.